JOURNAL OF GEOPHYSICAL RESEARCH, VOL. 106, NO. B4, PAGES 6595–6607, APRIL 10, 2001

The 1994 Java tsunami earthquake: Slip over a subducting seamount

Rachel E. Abercrombie, Michael Antolik, Karen Felzer, and Göran Ekström

Department of Earth and Planetary Sciences, Harvard University, Cambridge, Massachusetts

Abstract. On June 2, 1994, a large subduction thrust earthquake (M_S 7.2) produced a devastating tsunami on the island of Java. This earthquake had a number of unusual characteristics. It was the first recorded large thrust earthquake on the Java subduction zone. All of the aftershock mechanisms exhibit normal faulting; no mechanisms are similar to the main shock. Also, the large tsunami and the relatively low energy radiated by the main shock have led to suggestions that this earthquake might have involved slow, shallow rupture near the trench, similar to the 1992 Nicaragua earthquake. We first relocate the main shock and the aftershocks. We then invert long-period surface waves and broadband body waves to determine the depth and spatial distribution of the main shock slip. A dip of 12°, hypocenter depth of 16 km and moment of 3.5×10^{20} N m (M_w 7.6) give the best fit to the combined seismic data and are consistent with the plate interface geometry. The source spectrum obtained from both body and surface waves has a single corner frequency (between 10 and 20 mHz) implying a stress drop of ~0.3 MPa. The main energy release was preceded by a small subevent lasting ~12 s. The main slip occurred at ~20 km depth, downdip and to the NW of the hypocenter. This area of slip is collocated with a prominent high in the bathymetry that has been identified as a subducting seamount. We interpret the Java earthquake as slip over this subducting seamount, which is a locked patch in an otherwise decoupled subduction zone. We find no evidence for slow, shallow rupture. No thrust aftershocks are expected if the entire locked zone slipped during the main shock, but extension of the subducting plate behind the seamount would promote normal faulting as observed. It seems probable that such a source model could also explain the size and timing of the observed tsunami.

1. Introduction

The large earthquake (M_w 7.8 [*Dziewonski et al.,* 1995]) that occurred off the southern coast of Java, Indonesia, on June 2, 1994 exhibited a number of unusual characteristics. First, it is the only shallow thrust earthquake on the Java subduction zone in the Harvard centroid moment tensor (CMT) catalog (1976 to present [*Dziewonski et al.,* 1981; *Dziewonski and Woodhouse,* 1983; *Dziewonski et al.,* 1995]; the zone is dominated by normal faulting earthquakes (Figure 1a). Second, although the main shock is a shallow thrust earthquake, all of the aftershock CMT solutions are normal faulting mechanisms (Figure 1b). Third, it has been identified as a tsunami earthquake [*Newman and Okal*, 1998; *Polet and Kanamori*, 2000] because of the large amplitude of the tsunami compared with the earthquake magnitude. The tsunami killed over 250 people and had run-up heights reaching 14 m [*Tsuji et al.,* 1995].

The seismicity along the Java trench is low, dominated by normal faulting earthquakes in the subducting plate, and there are no previous large thrust earthquakes in the CMT catalog (Figure 1a). These observations suggest that the two plates are poorly coupled at the trench and that most subduction is by aseismic slip. The large number of extensional mechanisms also suggests a strong slab-pull force. This interpretation of the Java subduction zone is supported by the relatively old age (120-130 Ma) of the subducting seafloor [*Ruff and Kanamori,* 1980]. The occurrence of the June 1994 earthquake cast some doubt on this interpretation [*Chamot-Rooke and Le Pichon,* 1999]. It is possible for isolated locked patches to exist on otherwise decoupled subduction zones, which could slip in earthquakes. For example, *Lallemand and Le Pichon* [1987] proposed that such patches could be caused by the subduction of seamounts. *Masson et al.* [1990] mapped seamounts subducting at the Java trench using bathymetric and seismic data.

Tsunami earthquakes, which generate tsunamis significantly larger than predicted from their magnitude [*Kanamori,* 1972], are currently explained as having either an anomalous source process or being accompanied by slumping and underwater landslides. The 1992 Nicaragua earthquake is considered a classic example of the former [*Kanamori and Kikuchi*, 1993], and it has been suggested that the Java earthquake is also of this type [*Newman and Okal*, 1998; *Polet and Kanamori*, 2000]. The Nicaragua earthquake excited a large tsunami, and its seismic radiation was highly enriched at low frequencies [e.g., *Kanamori and Kikuchi,* 1993]. The anomalously large long-period energy implies that the earthquake had a long source duration. *Kanamori and Kikuchi* [1993] interpret this as resulting from the earthquake rupturing updip into a region where the plate interface is filled with soft subducted sediments. These would slow down the earthquake rupture front, resulting in a longer source duration and increasing the long-period radiation. Reliable estimates of the size of such an

Paper number 2000JB900403.
0148-0227/01/2000JB900403$09.00

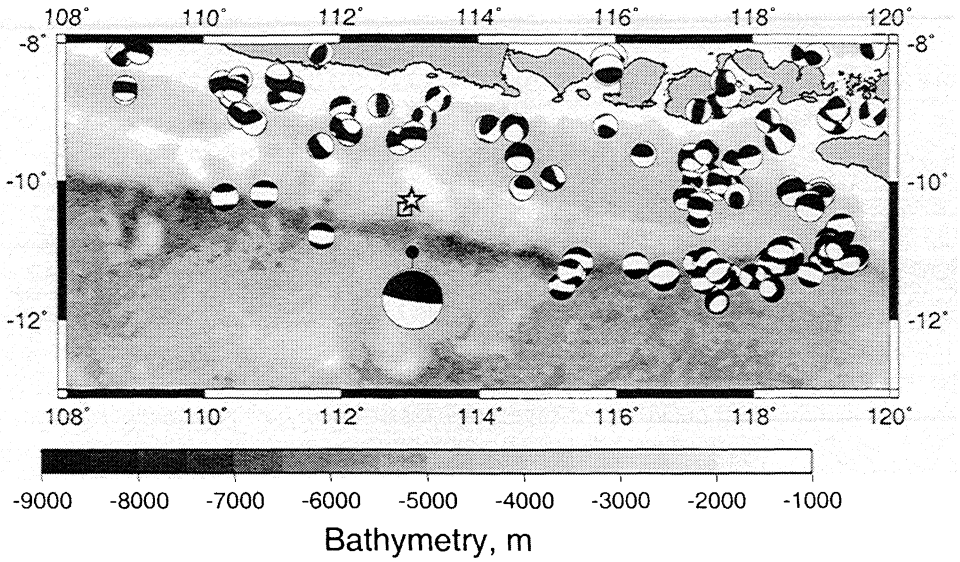

Figure 1a. Map of the earthquakes in the Harvard centroid moment tensor (CMT) catalog preceding the 1994 Java event. The bathymetry is shaded [from *Wessel and Smith,* 1991], and pale areas correspond to highs. Also shown are the locations of the 1994 Java earthquake by the International Seismological Centre (ISC, square), our relocation (star), and the Harvard catalog CMT centroid (solid circle).

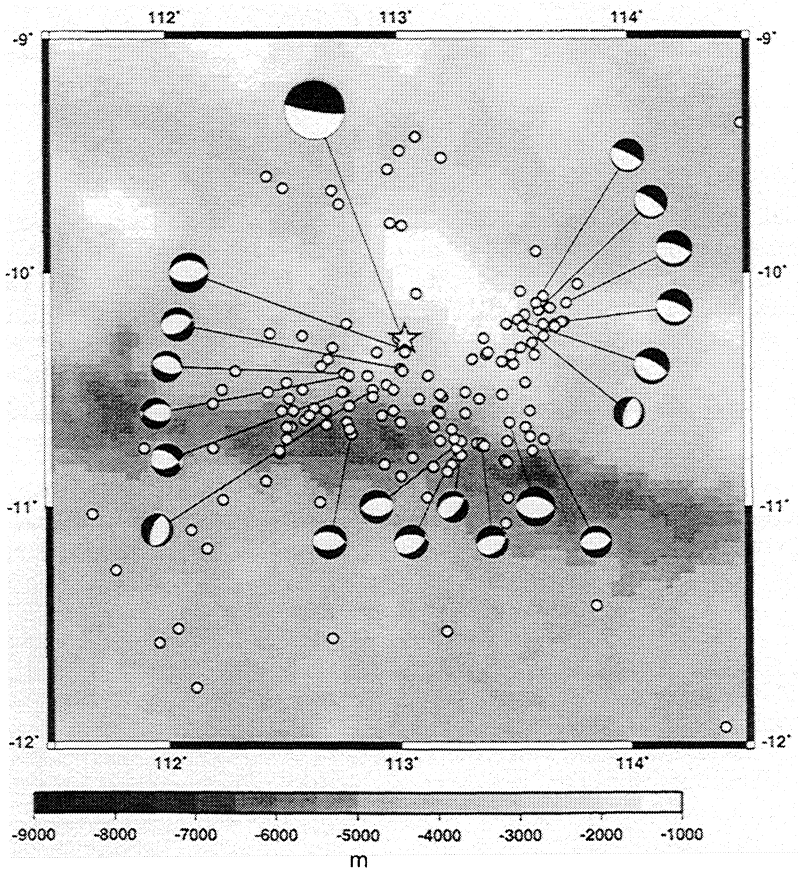

Figure 1b. Map of the relocated aftershocks (2 June to 22 October, 1994) of the 1994 Java earthquake. Also shown are all the CMT solutions in the Harvard CMT catalog. Note that the aftershocks appear to encircle the bathymetric high (pale area).

earthquake must be made at very long-periods (≥ 100 s), as conventional, higher-frequency magnitudes will both underestimate the true size of the earthquake and underpredict the amplitude of the resulting tsunami. *Newman and Okal* [1998] estimated the energy radiated by over 50 large earthquakes between 0.0143 and 2 Hz. They compared the energy with the seismic moments in the Harvard CMT catalog [*Dziewonski et al.,* 1981] that are determined for large earthquakes using data peaked at periods of 150 s (~7 mHz). *Newman and Okal* [1998] concluded that both the Nicaragua and Java earthquakes and a number of other tsunami earthquakes were significantly enriched in long-period energy, consistent with *Kanamori and Kikuchi's* [1993] hypothesis. *Polet and Kanamori* [2000] also compared relatively short period seismic energy measurements (1-20 s) with longer period seismic moment estimates and proposed a class of "slow tsunami earthquakes" consisting of the 1992 Nicaragua, 1994 Java, and 1996 Peru earthquakes. *Tanioka and Satake* [1996] modeled the tsunami from the 1994 Java earthquake. They found that the observed run-up heights were 30-50% greater than predicted by their model of slip in the upper 15 km of the plate interface, near the trench. This result included a contribution from horizontal displacement of the dipping ocean floor. Eye-witness reports of the arrival time of the tsunami, however, are inconsistent with a source near the trench and require it to be ~100 km closer to the coast, near the epicenter reported by the international agencies [*Tsuji et al.,* 1995].

We attempt to find a model for the Java 1994 earthquake that can explain its unusual characteristics. We first relocate the hypocenter of the main shock and aftershocks and the long-period centroid. We then perform broadband body wave modeling to constrain the depth and source mechanism. We also use a slip inversion method to improve the depth constraints and to investigate the lateral extent of the slip. This enables us to distinguish between a long source duration produced by a slow rupture velocity and one produced by a slow slip velocity with corresponding larger area, lower slip and lower stress drop. Although previous studies [e.g., *Newman and Okal,* 1998; *Polet and Kanamori*, 2000] using point source modeling have preferred the former, they were not able to distinguish between these two possibilities. We also investigate the shape of the long-period spectrum, in the range 2-20 mHz, between the frequency ranges previously studied. We then determine whether our source model is consistent with seismicity before and after the main shock, by modeling the static stress changes. Finally, we investigate whether our model can explain the observed tsunami.

2. Method

2.1. Relocation of the Hypocenter and Long-Period Centroid

Theoretically, the relative locations of the epicenter and the centroid of the moment in an earthquake can be used to indicate the direction of rupture propagation. Location errors in both measurements limit the resolution of this approach to only very large earthquakes [*Smith and Ekström,* 1997]. *Polet and Kanamori* [2000] used the relative locations of the International Seismological Centre (ISC) epicenter and the Harvard CMT centroid to infer updip propagation in the 1994 Java earthquake. We investigate the accuracy of the locations to determine if this approach is valid for this event. The ISC epicenter (Table 1), 50 km north of the trench, has small travel time residuals although the depth (39 km) is poorly constrained. We relocate the main shock hypocenter and all 184 aftershocks in the ISC catalog between June 2 and October 22, 1994, using a procedure which includes the effects of three-dimensional mantle velocity heterogeneity [*Smith and Ekström,* 1996]. We calculate the relocations using just *P* and both *P* and *S* picks and also compare locations with the depths free or held fixed at 39 km. Our preferred main shock epicenter is plotted in Figure 1 (Table 1). It is 65 km north of the trench and 19 km from the ISC location. Varying the depth has little effect on the epicenter but does result in a trade-off with the origin time. The aftershock epicenters (Figure 1b) are more tightly clustered following relocation, with lower residuals, although their average location changes little.

Table 1. Hypocentral Parameters for the June 2, 1994, Java Earthquake.

	Origin Time[a], s	Latitude, deg	Longitude, deg	Depth, km
ISC	37.01	-10.413	112.926	39.0
Relocation	39.0	-10.28	113.04	39.0[b]
CMT	36.8 (+ 39.0)	-11.03	113.04	15.0[b]

[a]Origin time is after 1817 UT and the CMT centroid time is included in parentheses.
[b]Depth was fixed.

The arrival time data are inadequate to provide useful constraints on the depths. If we assume that the main shock occurred at the plate interface, we can use the trench geometry to estimate the likely depth of the hypocenter. The Harvard CMT catalog solution for the main shock [*Dziewonski et al.,* 1995] has a poorly constrained dip of 7°. Assuming that the plate interface dips between 5° and 15°, the main shock hypocenter must have a depth between 6 and 17 km beneath the seafloor (Table 2).

The centroid location in the Harvard CMT catalog (Table 1 and Figure 1a) is to the south (seaward) of the epicenter and also the trench, which is inconsistent with faulting on the plate interface. This seems unlikely to be correct as the epicenter, mechanism and magnitude of the Java earthquake imply that it was probably on the plate interface. The centroid locations of 75% of the earthquakes along the Java trench in the Harvard CMT catalog are to the south of their ISC epicenters; half of them are more than 20 km apart, and the separation distances are independent of magnitude. This suggests that uncertainties in the Earth model used could cause the centroid locations to be systematically biased to the south. We therefore investigate the reliability of the centroid location. The depth and dip angle of shallow thrusts are not well constrained by long-period surface waves [*Kanamori and Given,* 1981; *Dziewonski et al.,* 1981], and so the depth was fixed in the catalog inversion. We try fixing the depth and dip at various values and reinverting for the CMT solution. Varying the depth from 10 to 25 km and the dip

Table 2. Constraints on the Dip and Depth of the Java Earthquake From Seismic Data and Plate Geometry.

Data	Dip, deg	Hypocenter Depth[a], km	Centroid Depth, km
Plate geometry	7[b]	8	-
Plate geometry	12[b]	14	-
Plate geometry	15[b]	17	-
CMT	7	-	13[b]
Broadband modeling	14	-	21
Broadband modeling	12[b]	-	19
Broadband onset modeling	12[b]	≥ 14	-
Slip inversion	12[b]	16	18-22

[a]All depths are below the seafloor assuming 2 km water depth. The plate geometry depths are obtained from the relocated epicenter.
[b]Parameter was fixed.

from 9° to 20° results in variations of only ±0.1° latitude, ±0.05° longitude, and ±1 s about the 38 s centroid time, implying that the centroid location is very stable. The strike and rake vary only by a few degrees, and the RMS misfit by <5%. The scalar moment, however, is inversely proportional to the dip, and increases from 3.5×10^{20} N m at 12° dip to 5.3×10^{20} N m at 7°.

In these inversions a preliminary reference Earth model (PREM) [*Dziewonski and Anderson,* 1981] crustal structure, 21 km thick, was assumed in the calculation of mode excitation. Recent work has shown that the crustal thickness has a large effect on the frequency spectrum of long-period surface waves [*Abercrombie and Ekström*, 2001]. Although the PREM crustal structure is probably a reasonable approximation for the Java main shock location, we also try inversions assuming a 6-km-thick ocean crust in the source region. The resulting centroid parameters are all within the range of previous inversions, and so we use the PREM structure in all subsequent modeling.

To investigate further what could be causing the earthquake centroid to locate south of the trench, we invert the mantle waves (long-period surface waves) and body waves separately to look for any systematic differences. The mantle wave solution is very similar to the one given in the catalog. The body waves alone do not converge to a good solution; the earthquake is really too large for a body wave solution. When the mechanism is fixed at the catalog CMT, the resulting centroid location is ~40 km north, and hence north of the trench, closer to the epicenter. This discrepancy between mantle and body wave solutions suggests that the three-dimensional velocity models used in the CMT inversion may be inadequate in an area of such complex tectonics. Thus we do not believe that the centroid location is to the south of the trench but that it is influenced by the same bias that was previously noted for the majority of the earthquake centroid locations on the Java trench. The relative locations of the epicenter and long-period centroid of the Java earthquake cannot therefore be used as reliable evidence of rupture updip toward the trench.

We thus constrain the epicenter to that in the ISC catalog. The long-period modeling limits the dip to between ~5° and 12°, and the centroid depth to between 10 and 20 km.

2.2. Broadband Body Wave Modeling

We model teleseismically recorded broadband body waves to improve the constraints on the depth and mechanism of the Java earthquake and to investigate the nature of the earthquake rupture propagation. The seismograms show that the earthquake began with a small subevent, lasting ~12 s. We investigate the rupture propagation during this subevent to constrain the relative locations of the hypocenter and the main energy release.

First, we model the whole earthquake using all the available recordings of both *P* and *SH* waves at Global Seismic Network (GSN) and Geoscope stations. We correct for the instrument responses to obtain displacement seismograms filtered between 1 and 500 s. We then invert for the moment tensor, source time function and depth using the method developed by *Ekström* [1989]. We use t^* of 0.6 s for *P* waves and 3.0 s for *S* waves. We use a layered velocity model over a half-space, with a 22 km crust (essentially PREM) and 2 km of water. The source is fixed at our relocated epicenter. Initially, we invert only *P* waves and predict the *S* waves to assist in correct picking of the *S* wave arrivals. The *P* wave inversion results in a depth of 16 km (below the sea surface, 14 km below the seafloor), and a pure reverse mechanism. We do not use the CMT solution as a significant constraint in the body wave inversion. The two mechanisms are very similar, but the body waves prefer a steeper dip of 13°. Addition of the *S* waves to the inversion results in a depth of 23 km and a dip of 14°. The strike and rake are very stable, and no non-double-couple component is required.

We then try inversions with fixed mechanisms, varying the dip, to obtain a fault plane orientation compatible with the CMT inversion results and also the geometry of the interface. We find that a dip of 12° gives the best fit to both the long-period and body wave data. Body wave modeling with this dip results in a depth of 21 km below the sea surface and a good fit to the seismograms. This preferred model is shown in Figure 2; it has a normalized residual variance of 0.3144, only 0.005 higher than the inversion with the free mechanism. This preferred source model is able to match the seismograms used in the CMT inversion, again with only a small, 5%, increase in misfit over the free inversion result. A dip of 12° and a depth below the seafloor of 19 km are also consistent with the geometry of the plate interface and the uncertainties in the epicenter. Decreasing the dip results in an increasingly poor fit to the broadband data, whereas increasing the dip results in an increasingly poor CMT solution. Our preferred model has a strike of 280°, a rake of 90°, and a dip of 12°. The dip errors can be no more than ~3°. The fit to the broadband body waves with this mechanism has a moment of 2.8×10^{20} N m, and a depth of 21 km. The source time function has a duration of 80 to 90 s and a centroid time of 39 s that is in good agreement with the CMT inversion result. Longer source time functions were allowed in the inversion but were not required.

We also include directivity in the inversions, but it is negligible (≤0.5 km/s). The station distribution, with few stations to the south, is not ideal for identifying directivity, but it is adequate to rule out strong rupture propagation effects.

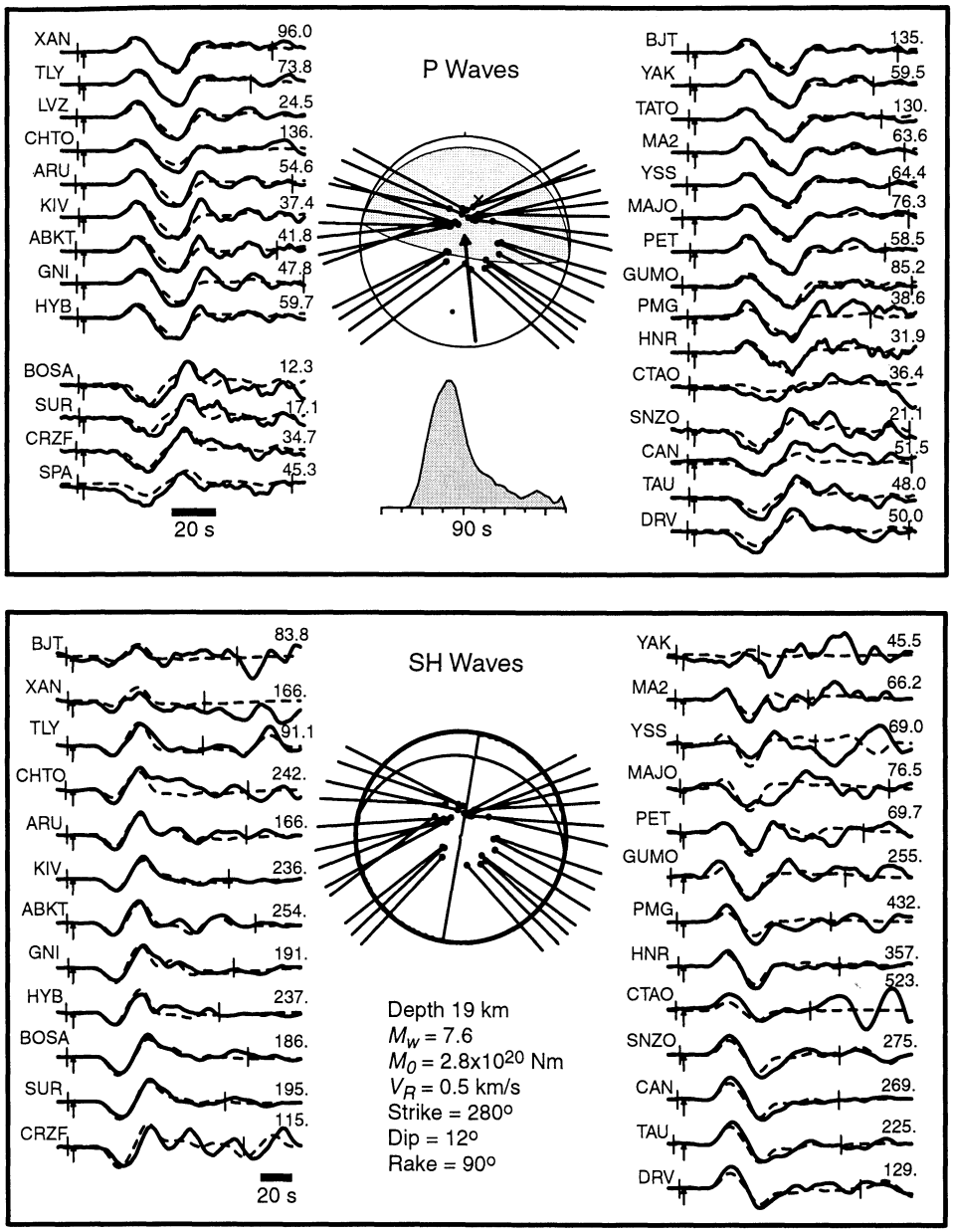

Figure 2. Broadband body wave modeling of the main shock, showing the observed seismograms (solid) and synthetics (dashed) for our preferred model. The vertical lines on each seismogram indicate the time window used in the inversion. The vertical arrows are the picked onsets. The numbers to the right of the seismograms are the maximum amplitude in microns. The arrow on the focal mechanism indicates the direction of rupture propagation.

The seismograms and the source time function (Figure 2) all have relatively low-amplitude onsets, suggesting that the rupture initiated with a small subevent. The main energy release begins 12-14 s after the origin time. The inversions for the entire source process give little weight to this small onset, and so to investigate rupture propagation prior to the main slip, we invert separately the first 10-12 s of the *P* wave seismograms. As we are not including all the depth phases from the initial rupture (because they are obscured by later, much larger arrivals) we cannot constrain both the mechanism and depth. We therefore fix the mechanism at our preferred model and invert for the source time function at various fixed depths. We use the 16 stations with the highest signal to noise ratio (Figure 3). We cannot obtain an acceptable fit with the depth <15 km beneath the sea surface, and the fit improves with increasing depth to 20 km (Figure 3). Thus the initial depth could be the same as that of the centroid. Repeating the exercise with a smaller dip of 7° resulted in higher misfit at almost all depths. The moment in the first 11 s appears to be divided into two subevents and totals about 9×10^{17} N m, which is ~0.25% of the total moment of the earthquake. Such small initial subevents are relatively

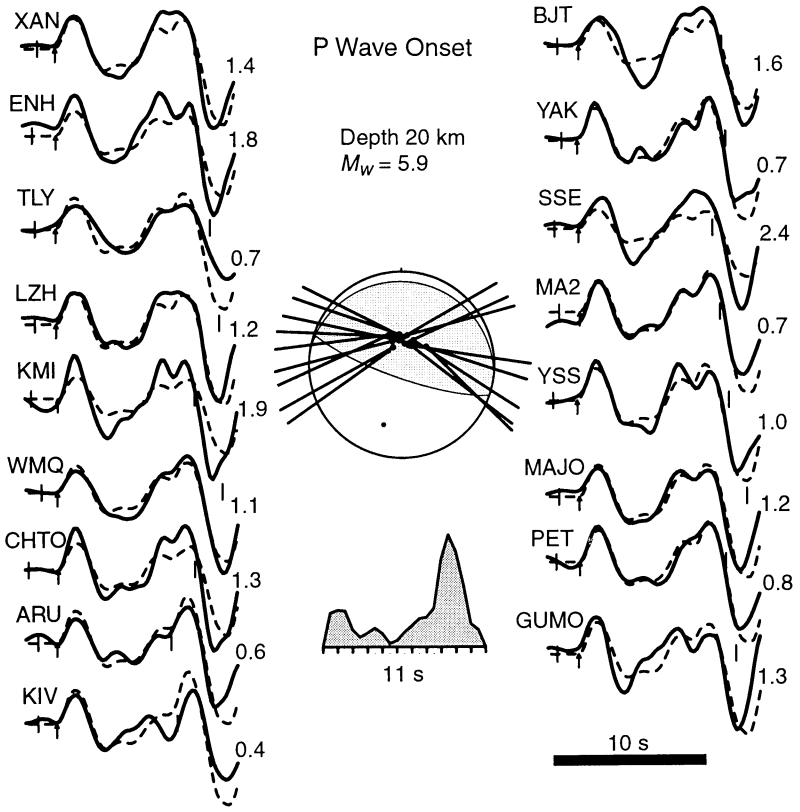

Figure 3. Broadband body wave modeling of the onset of the main shock at selected stations. The mechanism is fixed, and a depth of 20 km gives the best fit. See Figure 2 for explanation of symbols

common [e.g. *Abercrombie and Mori,* 1994; *Ellsworth and Beroza,* 1995] and represent either early subevents in a cascading rupture or possibly a late stage in a poorly understood nucleation process.

We also search for any evidence of rupture propagation during these early stages. No depth change between the hypocenter and the onset of the main energy release is required. We include directivity in our modeling of the onset, but the maximum rupture velocity obtained was 0.6 km/s, to the NNE. Constraining the solution to a point source produced a negligible increase in misfit. No evidence of rupture updip (to the south) was observed. We also try simply measuring arrival times of distinctive early phases at different stations. There is some suggestion that the main energy release starts later at the southern stations CAN and DRV but only by 0.6 s. As noted above, the station distribution is not good for resolving rupture directivity, but substantial rupture propagation would be identifiable. For example, the 1994 Romanche earthquake (M_w 7.0) had a similar duration small onset but showed strong directivity in the early stages [*Abercrombie and Ekström,* 2001]. For that earthquake the relative arrival time of the main energy release varied with azimuth by 4 s. Therefore we think it is safe to conclude that little unilateral rupture propagation occurred within the first 10 to 15 s of the Java earthquake, and the onset of the main energy release was very close to the hypocenter.

2.3. Finite Fault Slip Inversion

We perform a finite fault slip inversion to investigate the slip distribution during the Java earthquake and to determine the location of the main energy release. The seismograms used are essentially the same as those used in the broadband body wave modeling, without the high pass filter. In addition, for the slip inversion we decimate the sampling rate to 1 sample/s. We invert a total of 35 *P* and *S* body wave records from 26 stations (see Figure 4). We use the method described by *Antolik et al.* [2000], developed from that of *Hartzell and Heaton* [1983]. In the inversion the chosen fault plane is divided into a grid of 5 × 5 km subfaults. Whole Earth synthetic seismograms for each subfault are computed using the reflectivity method and a layered representation of the IASPEI91 velocity model. A layered attenuation model is also included [*Durek and Ekström,* 1996]. The rupture front is forced to propagate at a constant rupture velocity across the fault plane, and the source time function for each subfault is an isosceles triangle of fixed duration. We obtain a solution by using damped least squares with a positivity constraint on the moment release.

We fix the fault plane orientation to that in our preferred model with a dip of 12°. We also try inversions with a dip of 7°, but these consistently produce poorer fits. We fix the hypocenter at 16 km beneath the seafloor, consistent with the broadband modeling and the subduction zone geometry. If we begin the inversion at the origin time, a very low rupture velocity is required to fit the seismograms (~1 km/s). This is consistent with the broadband modeling result that the rupture moved little in the first 12 to 14 s. We therefore add a delay to the beginning of the slip model, as the initial slip is too small to be resolved in the inversion. We vary the rupture velocity and delay to find the preferred velocity and to allow

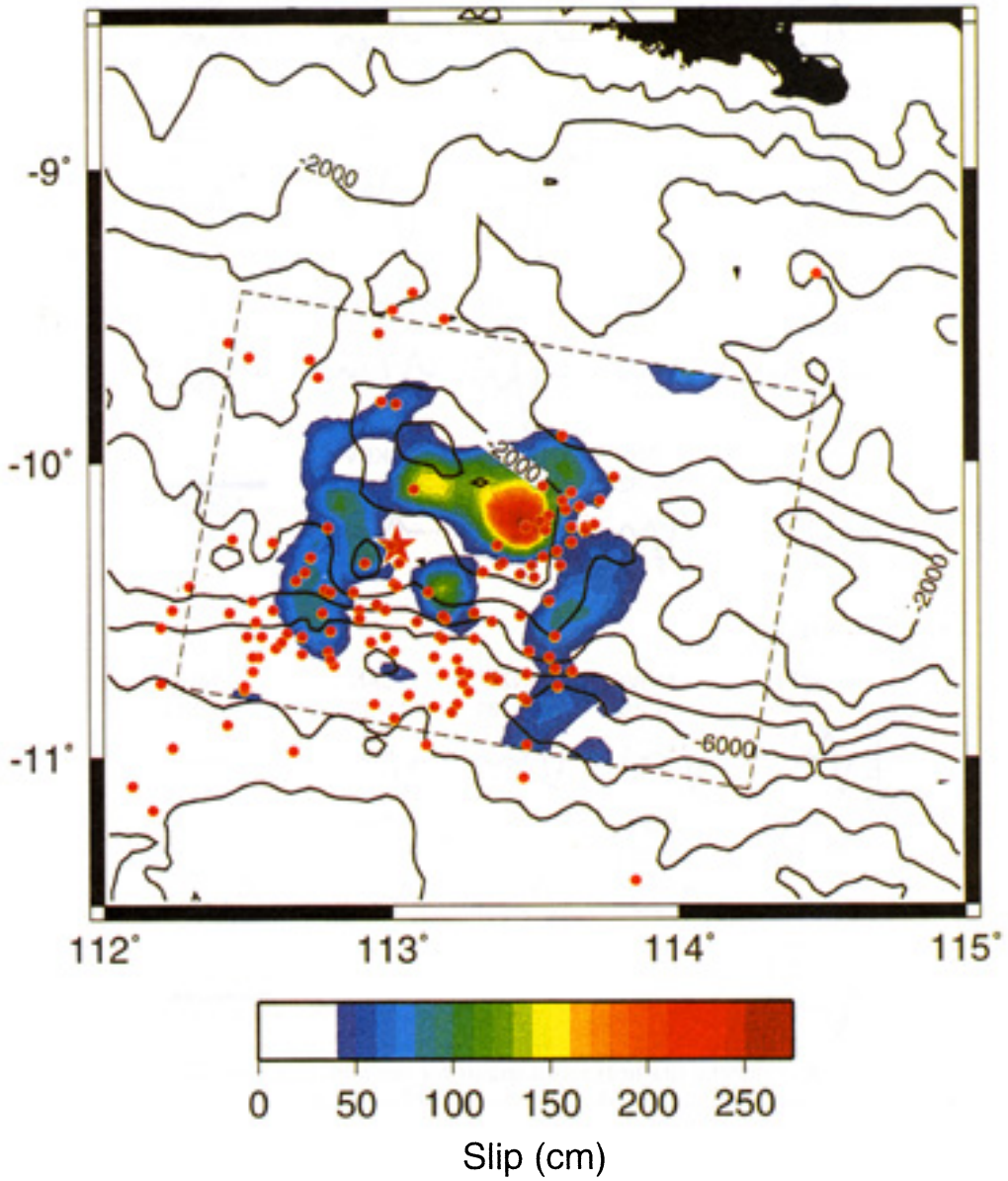

Plate 1. Slip inversion result for our preferred model, projected to the horizontal, and overlain by the bathymetry. The red star is the relocated epicenter, and the aftershock relocations are shown as red circles. The dashed line indicates the size of fault used in the slip inversion, the top is at a depth of 1.7 km. The area of principal slip corresponds to the bathymetric high.

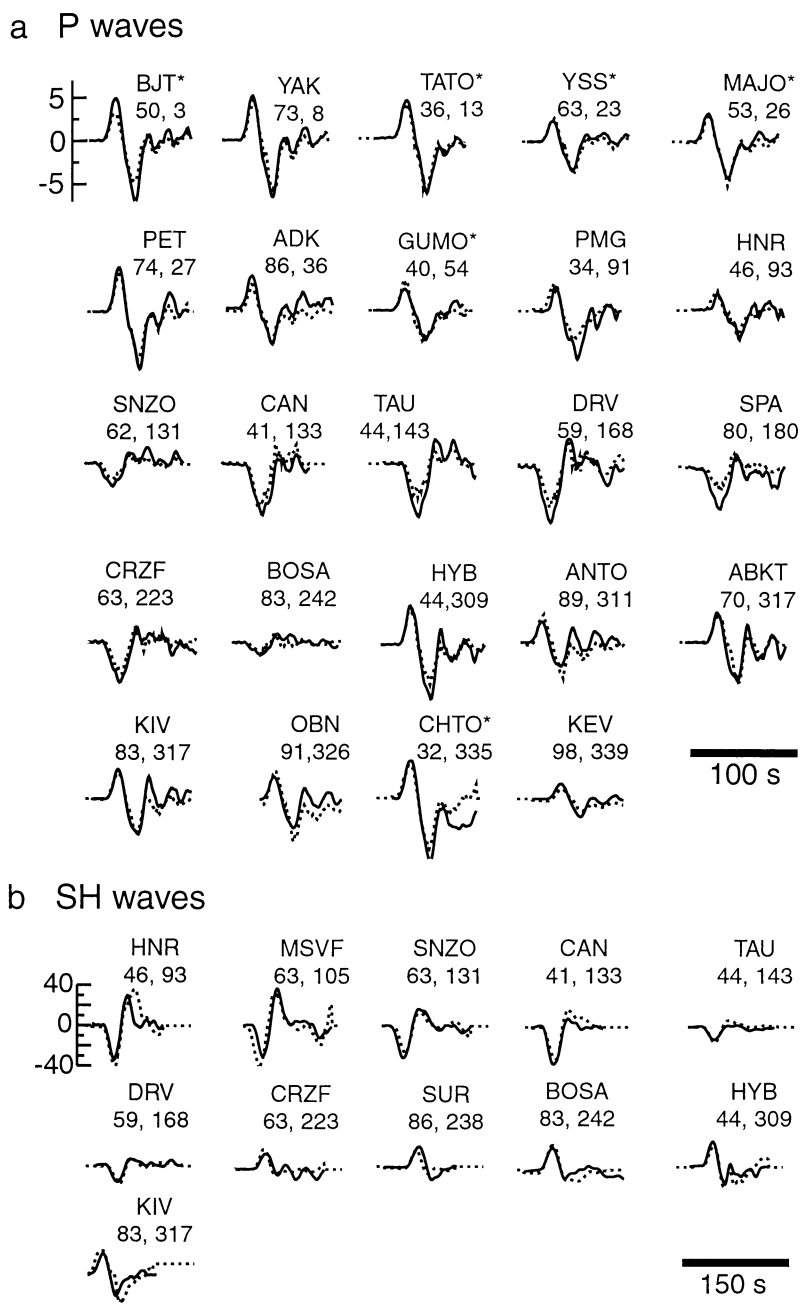

Figure 4. Observed (solid) and synthetic (dashed) seismograms for our preferred slip inversion. The amplitudes are in 10^{-5} m, but stations indicated with an asterisk are plotted at 50% of the actual amplitude for (a) *P* waves and (b) *SH* waves.

for some movement between the hypocenter and the main energy release.

The robust feature of all the models is the patch of slip to the ENE of the hypocenter, ~40 by 80 km (Plate 1). This corresponds to the large pulse peaking at ~30 s in the source time function (Figure 2). A delay of 12 s and a rupture velocity of 2 km/s (~0.6 V_S) give the best fit to the data with a reasonable slip distribution. The peak slip is 2.5 m.

The location of the peak slip is well constrained in both lateral position and depth. Altering the rupture velocity, or the hypocenter and dip of the fault plane so as to exclude slip at this location produced very poor fits to the seismograms and unrealistic slip distributions. No evidence for any significant rupture updip from the hypocenter was found. We can therefore constrain the principal slip to have occurred in the depth range 18 to 22 km and between 30 and 70 km to the east and downdip of the hypocenter. The area of maximum slip is coincident with a large bathymetric high, north of the trench (Plate 1). This feature has been mapped as a subducting seamount by *Masson et al.* [1990].

2.4. Long-Period Spectrum

The shape of the earthquake source spectrum has been used to identify slow and tsunami earthquakes [e.g., *Ihmlé*, 1996; *Polet and Kanamori,* 2000]. We can obtain the source spectrum at long-periods using the CMT inversion procedure.

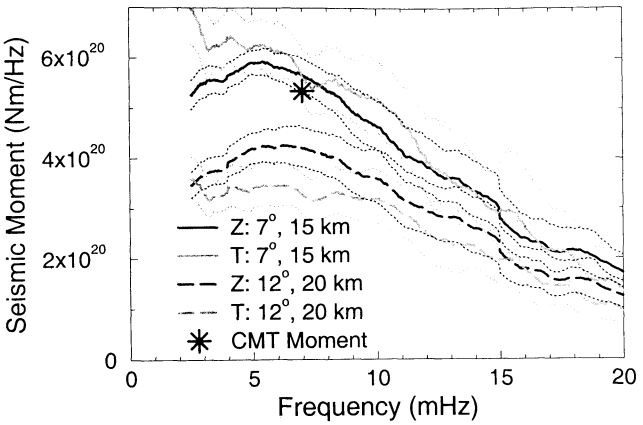

Figure 5. Long-period (mantle wave) source spectrum. The solid curves are for a dip of 7° and the dashed for a dip of 12°. The solid curves are for the vertical (Rayleigh) waves, and the shaded curves are for the transverse (Love) waves. The star marks the Harvard CMT catalog moment.

Combining this with the spectrum of the source time function obtained at shorter periods from the body waves enables us to obtain a more complete picture of the spectrum than has been calculated previously [*Newman and Okal,* 1998; *Polet and Kanamori,* 2000].

The source spectrum is essentially the spectrum of the recorded seismogram divided by that of a synthetic Green's function, which accounts for the source orientation and position, and wave propagation effects. We have developed a method that uses the CMT inversion procedure to produce synthetic seismograms for a point source of prescribed position and orientation, with a delta function (0.5 s) duration. We then calculate spectral ratios of the observed and synthetic spectra at each station, in the frequency range where there is good signal. We average over all available stations to obtain a source spectrum [*Abercrombie and Ekström,* 2001]. Figure 5 shows the source spectra calculated for the catalog CMT solution and also for our preferred model with a dip of 12°. The dip has a significant effect both on the total moment and on the shape of the resulting source spectrum. Varying the depth of the source also affects the shape of the spectrum, but for a shallow thrust source mechanism the effect is relatively minor. It is smaller and of an opposite nature to that observed for strike slip faults [*Abercrombie and Ekström,* 2001]. We also investigate whether directivity affects the shape of the source spectrum by calculating the spectrum for stations at different azimuths, but we find it to have a relatively small effect.

We then combine our preferred long-period source spectrum (the average of the vertical and transverse components) with that of the source time function obtained from the slip inversion, and also the spectral measurements made by *Polet and Kanamori* [2000]. The spectra are remarkably consistent and the combined spectrum exhibits a single corner frequency of 10-20 mHz (Figure 6a). The good agreement between the spectra obtained from the broadband body waves and the long-period surface waves implies that no significant long-period radiation was produced by slow slip that was not included in the body wave modeling.

2.5. Aftershocks and Static Stress Modeling

The aftershocks of the Java earthquake cluster to the south and east of the epicenter (Figure 1b) and appear to surround both the area of principal slip (Plate 1) and the bathymetric high with which it is associated. CMT solutions are available for the 19 largest aftershocks (M_w 5.2 to 6.6), which occurred within the first month, all of which exhibit normal faulting (Figure 1b). The aftershocks appear to fill a gap in the background seismicity. Although normal faulting earthquakes were distributed along the trench, prior to the Java earthquake none occurred to the south of the bathymetric high (Figure 1a).

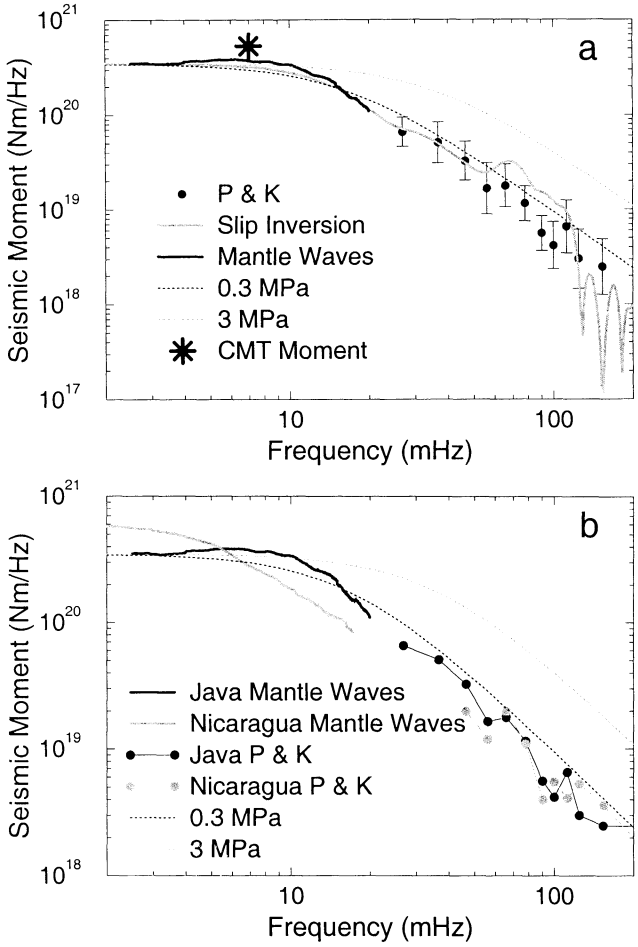

Figure 6. (a) The source spectrum of our preferred long-period source spectrum (12° dip, mean of Z and T components), combined with the measurements of *Polet and Kanamori* [2000], (P & K) and the spectrum of the source time function obtained from the slip inversion. Error bars are omitted from the mantle wave spectrum for clarity. The star marks the Harvard CMT Catalog moment. The theoretical curves for stress drops of 0.3 and 3 MPa are calculated assuming a *Brune* [1970] spectral model, following *Polet and Kanamori* [2000]. (b) Comparison of the source spectra of the 1994 Java earthquake with that of the 1992 Nicaragua earthquake. The long-period mantle wave spectra are calculated in this study and combined with the body wave spectra determined by *Polet and Kanamori* [2000], (P & K). The error bars are omitted for clarity but are of similar size to Figures 5 and 6a.

The CMT solutions of the aftershocks fall into two distinct groups. The aftershocks to the south of the epicenter are on normal faults striking roughly east-west and dipping at ~45°. The group of aftershocks to the east of the epicenter is characterized by a shallow nodal plane dipping to the south and a steep one dipping to the north. Their strikes are also rotated to be more trench parallel than the southerly aftershocks. The two groups of aftershocks are also separated in time; activity to the south began immediately after the main shock, but the main activity in the eastern group of aftershocks occurred more than 10 days later.

The epicenters of the aftershocks are well constrained, but the depths are poorly known. They are all shallow, but the relocation procedure does not constrain the depths well. Preliminary broadband modeling of three aftershocks confirms the two types of normal mechanism and provides some evidence that the aftershocks south of the main shock are shallower (~15 km) than the ones to the east (~30 km). If this is the case, then all of the aftershocks probably represent extension in the subducting plate. None of the largest aftershocks involve reverse motion, nor are they likely to have occurred on the plate interface.

It has now become common practice to calculate the static stress changes produced by a large earthquake and to relate these changes to the distribution of aftershocks [e.g. *Stein,* 1999]. *Gomberg and Ellis* [1994] developed a three-dimensional method, based on the model and programs of *Okada* [1992], which we use to calculate static stress changes for a simplified version of our slip model embedded in a half-space. The lack of good depth constraints for the aftershocks limits our resolution. Also, the slip distribution produces a heterogeneous spatial distribution of stress change. The models do predict a decrease in failure stress to the south of the main shock, and so those earthquakes are likely to be consistent with such a model. This makes good sense, as slip on the interface would be expected to produce extension in the outer rise. The aftershocks to the east, however, are in a region where stress could have increased or decreased depending on their precise location and depth relative to the main shock slip distribution.

Nevertheless, we can conclude that the occurrence of normal faulting aftershocks is roughly consistent with the static stress changes produced by the main shock. The static stress models also predict similar sized decreases in failure stress on faults orientated for reverse slip, and so they cannot explain the conspicuous absence of any reverse faulting aftershocks.

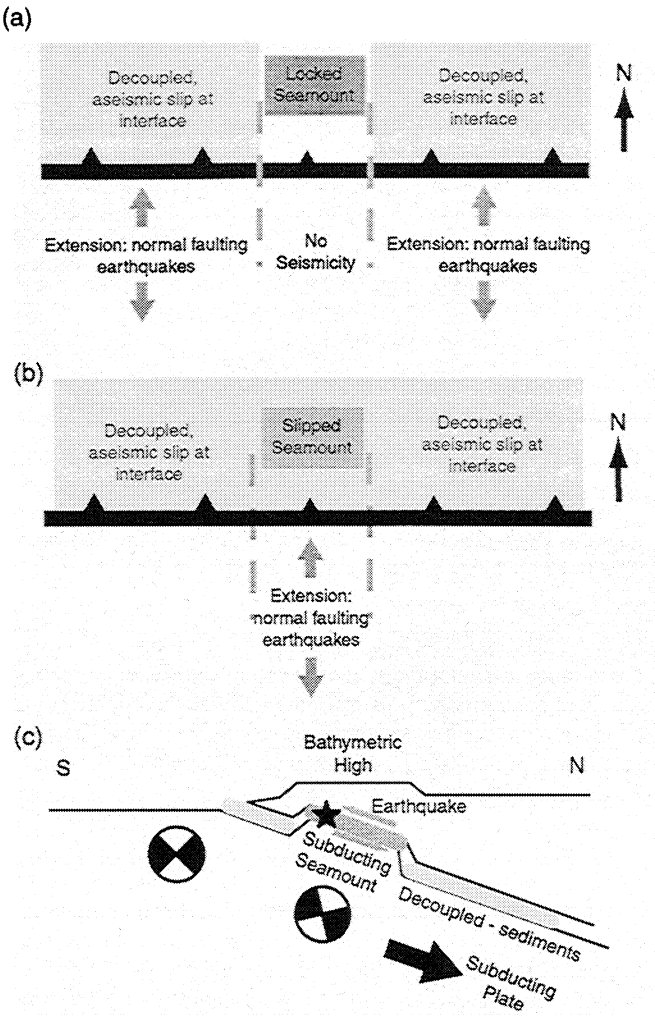

Figure 7. Cartoon depicting our model of the Java earthquake and the seismicity along the Java trench. (a) Before the Java earthquake. The subducted seamount is a locked patch on an otherwise decoupled, aseismically slipping interface. This aseismic subduction causes extension in the outer rise, and hence normal faulting earthquakes. These are absent behind the subducting seamounts where the plate is not slipping. (b) The Java earthquake rupturing the locked patch. This causes extension in the outer rise behind the subducted seamount and consequently normal faulting aftershocks. The normal faulting seismicity along the rest of the trench will continue as before. (c) A cross section of our model. The star indicates the hypocenter. The darker shading represents the area ruptured in the Java earthquake, and the lighter shading, areas where sediments weaken the interface, allowing aseismic slip. The focal mechanisms are typical of the two groups of aftershocks, representing extension in the subducting plate following slip over the locked seamount.

3. Results and Discussion

3.1. Slip Over a Subducting Seamount

Our preferred model of the Java earthquake, which appears best suited to explain the diverse observations, is that the earthquake involved slip on a locked patch within a decoupled subduction zone that is slipping aseismically. Low coupling is predicted from the old age of the subducting plate (120-130 Ma) [*Ruff and Kanamori,* 1980]. Also, the background seismicity pattern, with no plate-interface thrust earthquakes but numerous normal events in the outer rise, suggests that aseismic subduction is occurring along much of the trench and causing extension in the outer rise. The lack of normal faulting earthquakes at some locations along the trench suggests that in these localities the plate interface is locked (Figure 1a). *Masson et al.* [1990] identified a number of subducting seamounts from bathymetric and seismic studies of the Java trench in the Java trench. The subducting seamounts are located at approximately 108.5°, 111.1°, 111.5°, 113°, 114.8°, and 118.5-119° east. Many are associated with highs in the bathymetry (Figure 1a). The seamount farthest to the east coincides with the seismicity associated with the Sumbawa Island earthquake (M_w 8.3,

1977). The others correspond roughly to gaps in the pattern of normal earthquakes, suggesting that they are places where the trench is locked.

The focal mechanism and epicenter location of the Java earthquake imply that it involved slip on the plate interface. The location of the principal slip is tightly constrained by the body wave modeling and slip inversion. It coincides with the seamount at 113°E identified by *Masson et al.* [1990]. We conclude that the earthquake involved slip over the subducting seamount in a locally well-coupled part of the interface. If the interface surrounding the seamount is not well coupled, then reverse-faulting aftershocks would not be expected on the interface. The main shock slip would produce localized extension in the outer rise, however, and so explain the normal faulting aftershocks. This model of the seismicity along the Java trench is shown in cartoon form in Figure 7.

The effect of subducting seamounts on the seismic coupling at subduction zones and the consequences for earthquake recurrence have been studied by various authors, for example, *Lallemand and Le Pichon* [1987] and *Scholz and Small* [1997]. *Scholz and Small* [1997] calculated that the subduction of a large seamount would increase the normal stress on the interface. This could lead to locally locked patches on an otherwise decoupled, aseismically slipping subduction zone. They found their model to be consistent with the occurrence of two large earthquakes on the Tonga subduction zone. It also seems a plausible model for the 1994 Java earthquake.

3.2. Was the Java Earthquake a "Slow" Earthquake?

Our composite source spectrum of the Java earthquake is shown in Figure 5(a). It has a single corner frequency between 10 and 20 mHz. The total moment, 3.5×10^{20} N m, is slightly lower than that in the CMT catalog because of the steeper dip of our preferred mechanism.

We can use the slip distribution and long-period spectrum to estimate the stress drop in the earthquake. For a dip-slip earthquake of length L and width W, the stress drop,

$$\Delta\sigma = C\frac{M_0}{W^2 L},$$

after *Kanamori and Anderson* [1975], where the factor $C \sim 1$. The total rupture length from the slip distribution of the Java earthquake (Figure 5) is about 160 km, the width is about 80 km, and $M_0 = 3.5. \times 10^{20}$ N m, giving $\Delta\sigma \sim 0.3$ MPa. Uncertainty in the minimum resolvable slip used to estimate the area affects these estimates by about 10%. The 80 s duration of the source time function, at a rupture velocity of 2 km/s, also gives a length of 160 km. This duration and stress drop are in good agreement with the source spectrum, which is well fit by a theoretical model with a 0.3 MPa stress drop (Figure 6a). This stress drop is an average for the whole earthquake. If we only consider the principal area of slip ($L \sim$ 80 km, $W \sim$ 40 km, Plate 1) we obtain a stress drop of ~3 MPa.

These stress drops are lower than average global values but are well within the commonly observed variation [e.g., *Kanamori and Anderson*, 1975; *Abercrombie,* 1995]. If the rigidity is relatively low, as has been suggested for regions of sediment subduction [*Satake,* 1994], then the estimates of slip and stress drop for the Java earthquake will be underestimates. Alternatively, if the rupture area includes decelerating slip as the rupture propagated beyond the edges of the locked zone before stopping, then the average stress drop would be reduced. *Houston* [1990] and *Choy and Boatwright* [1995] have found that subduction zone thrust earthquakes often have relatively low apparent stresses, an alternative measure of stress drop, compared to the global average.

Figure 6b compares the spectrum of the Java earthquake with that obtained in a similar manner for the Nicaragua earthquake. At high frequencies the spectra of the two earthquakes are indistinguishable [*Polet and Kanamori,* 2000], but below ~20 mHz they differ significantly. The spectrum of the Java earthquake has a single corner frequency between 10 and 20 mHz and is flat at lower frequencies. The Nicaragua earthquake spectrum exhibits a corner between 3 and 4 mHz, but then a second corner is required between ~20 and 40 mHz to match the extrapolations of the high- and low-frequency spectra. This view of the Nicaragua earthquake spectrum agrees with that of previous workers [*Ihmlé,* 1996; *Kanamori and Kikuchi,* 1993]. It is also consistent with the Java earthquake having a larger moment than the Nicaragua earthquake in the Harvard CMT catalog since those moments are measured at ~ 7 mHz [*Dziewonski et al.,* 1981].

These differences are consistent with the interpretation of the Nicaragua earthquake as a compound event, involving an ordinary earthquake with a moment of $\sim 10^{20}$ N m, combined with an anomalously slow source lasting over 100 s, with a moment of $\sim 4 \times 10^{20}$ N m. Such a compound model is not required to explain the observations of the Java earthquake. There is no evidence for such an anomalously slow rupture component. Instead, the Java earthquake appears well explained as a single, ordinary velocity earthquake with a low stress drop.

Polet and Kanamori [2000] proposed a category of "slow tsunami earthquakes" that radiate excess long-period energy and cause large tsunamis as a result of slow, shallow slip near the trench. They characterized these earthquakes using a number of factors including (1) a long duration implying slow rupture velocity with relatively low energy release at high frequencies, (2) rupture propagation updip to shallow depth, (3) a high percentage of normal faulting aftershocks, and (4) a small accretionary prism and evidence of a subducting sedimentary layer. The *Polet and Kanamori* [2000] model appears to explain the 1992 Nicaragua earthquake well, but it is less appropriate for the Java earthquake. It fails to explain a number of differences between these two earthquakes. Seismicity along the Nicaragua trench is dominated by reverse faulting earthquakes unlike the Java trench. The subducting plate at Nicaragua is younger (20-30 Ma) than that at Java, which implies a higher degree of coupling at the plate interface. The Nicaragua earthquake had an unusually high proportion of normal faulting aftershocks, but the majority of the aftershocks had reverse mechanisms, in contrast to the absence of reverse faulting aftershocks following the 1994 Java earthquake. The lack of excess long-period energy and updip propagation at Java also render the *Polet and Kanamori* [2000] model inappropriate for the 1994 Java earthquake.

3.3. Generation of the Large Tsunami

If the Java earthquake did not involve large slip and slow rupture propagation at shallow depths how can we explain the

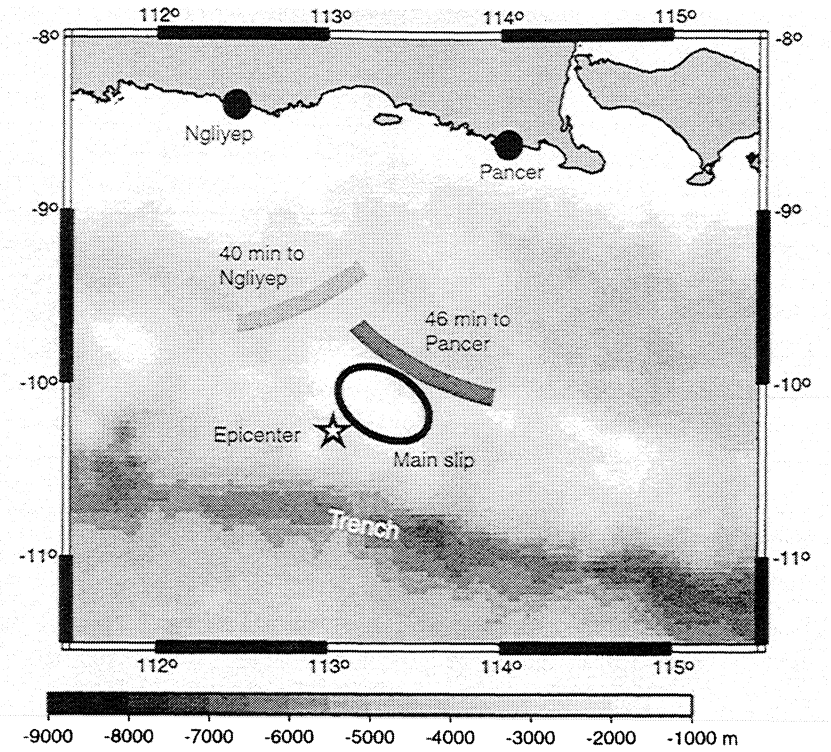

Figure 8. Map after *Tsuji et al.* [1995] showing the predicted source origin of the tsunami based on eyewitness reports in the towns of Ngliyep and Pancer. The time from Pancer is thought to be the most reliable.

large tsunami? First, the tsunami from the Java earthquake was only 30-50% larger than that predicted by numerical modeling [*Tanioka and Satake,* 1996], unlike the Nicaragua earthquake where the tsunami was an order of magnitude larger than predicted [*Satake,* 1994]. It was therefore probably within the uncertainties in the observations (run-up heights only, there are no tide gauge records) and the modeling. We plot the predicted origin of the tsunami in Figure 8, after *Tsuji et al.* [1995]. The timing of the Java tsunami is inconsistent with an origin near the trench, unlike that of the Nicaragua earthquake [*Satake,* 1994]. Only eyewitness reports of the arrival time are available, but they would have to be consistently 10 to 15 min early to agree with a tsunami originating at the trench. The reported times are in excellent agreement with an origin near our preferred location of principal slip, at the bathymetric high (Figure 8).

Whether our proposed source model could generate the observed tsunami cannot be determined without further tsunami modeling. Several factors suggest that it is possible, however. *Tanioka* [1999] tried several earthquake slip models with the same total moment to match the tsunami of the 1998 Papua New Guinea earthquake. One model involved shallow slip near the trench, similar to the modeling of the Java tsunami [*Tanioka and Satake,* 1996], and a second involved deeper slip over a smaller area, nearer to the coast. This latter model is similar to our proposed source model of the Java earthquake. *Tanioka* [1999] found that this model produced tsunami amplitudes several times as large as those generated by the shallow slip model at distant tide gauges. In addition, horizontal displacement of the steep slopes surrounding the bathymetric high, combined with the likelihood of slumping on the same slopes, would also increase the size of the observed tsunami. We therefore think that our preferred source model provides a plausible explanation for the observed tsunami.

4. Conclusions

Our principal conclusion, based on analysis of a wide range of data, is that the 1994 Java earthquake resulted from slip on a locked patch within an otherwise decoupled subduction zone. The rupture area corresponds to the location of a subducting seamount.

The distribution of background seismicity prior to the earthquake, as well as the unusual aftershock sequence consisting solely of normal faulting earthquakes, are consistent with the stress changes predicted by this source model. The source spectrum determined between 2 and 200 mHz has a single corner frequency (between 10 and 20 mHz) and, combined with the slip distribution, implies a relatively low average stress drop of 0.3 MPa. There is no evidence for anomalously slow slip or for shallow rupture near the trench.

The 1994 Java and 1992 Nicaragua earthquakes had significantly different source processes, despite their both having low ratios of energy to moment. The Java earthquake did not include a slow component of rupture of the kind observed for the 1992 Nicaragua earthquake.

Acknowledgments. We are grateful to J. Polet for providing her source spectrum and also for sending us a preprint of her paper. We use the GMT software for many of the figures [*Wessel and Smith,* 1991]. We thank M. Nettles for helpful comments on an earlier version of this manuscript. Reviews by H. Houston, J. Revenaugh, and an anonymous reviewer significantly improved the text. This work was funded by NSF award EAR-98-05172.

References

Abercrombie, R. E., Earthquake source scaling relationships from -1 to 5 M_L, using seismograms recorded at 2.5 km depth, *J. Geophys. Res., 100,* 24015-24036, 1995.

Abercrombie, R. E., and Ekström, G., Earthquake slip on oceanic transform faults, *Nature*, in press, 2001.

Abercrombie, R. E., and J. Mori, Local observations of the onset of a large earthquake: 28 June 1992, Landers, California, *Bull. Seismol. Soc. Am., 84,* 725-734, 1994.

Antolik, M., A. Kaverina, and D. Dreger, Compound rupture of the great 1998 Antarctic plate earthquake, *J. Geophys. Res., 105,* 23,825-23,838, 2000.

Brune, J. N., Tectonic stress and the spectra of seismic shear waves from earthquakes, *J. Geophys. Res., 75,* 4997-5009, 1970.

Chamot-Rooke, N., and X. Le Pichon, GPS determined eastward Sundaland motion with respect to Eurasia confirmed by earthquakes slip vectors at Sunda and Philippine trenches, *Earth Planet. Sci. Lett., 173,* 439-455, 1999.

Choy, G. L., and J. L. Boatwright, Global patterns of radiated seismic energy and apparent stress, *J. Geophys. Res., 100,* 18,205-18,228, 1995.

Durek, J. J., and G. Ekström, A radial model of anelasticity consistent with long-period surface wave attenuation, *Bull. Seismol. Soc. Am., 86,* 144-158, 1996.

Dziewonski, A. M., and D. L. Anderson, Preliminary reference earth model (PREM), *Phys. Earth Planet. Inter., 25,* 297-356, 1981.

Dziewonski, A. M., and J. H. Woodhouse, An experiment in systematic study of global seismicity: Centroid moment tensor solutions for 201 moderate and large earthquake of 1981, *J. Geophys. Res., 88,* 3247-3271, 1983.

Dziewonski, A. M., T.-A. Chou, and J. H. Woodhouse, Determination of earthquake source parameters from waveform data for studies of global and regional seismicity, *J. Geophys. Res., 86,* 2825-2852, 1981.

Dziewonski, A. M., G. Ekström and M. P. Salganik, Centroid-moment tensor solutions for April - June 1994, *Phys. Earth Planet. Inter., 88,* 69-78, 1995.

Ekström, G., A very broadband inversion method for the recovery of earthquake source parameters, *Tectonophysics, 166,* 73-100, 1989.

Ellsworth, W. L., and G. C. Beroza, Seismic evidence for an earthquake nucleation phase, *Science, 268,* 851-855, 1995.

Gomberg, J., and M. Ellis, Topography and tectonics of the New Madrid seismic zone: Results of numerical experiments using a three-dimensional boundary element program, *J. Geophys. Res., 99,* 20,299-20,310, 1994.

Hartzell, S., and T. H. Heaton, Inversion of strong ground motion and teleseismic waveform data for the fault history of the 1979 Imperial Valley, California, earthquake, *Bull. Seismol. Soc. Am., 73,* 649-674, 1983.

Houston, H., Broadband source spectrum, seismic energy, and stress drop of the 1989 Macquarie Ridge earthquake, *Geophys. Res. Lett., 17,* 1021-1024, 1990.

Ihmlé, P. F., Monte Carlo slip inversion in the frequency domain: Application to the 1992 Nicaragua slow earthquake, *Geophys. Res. Lett., 23,* 913-916, 1996.

Kanamori, H., Mechanism of tsunami earthquakes, *Phys. Earth Planet. Inter., 6,* 246-259, 1972.

Kanamori, H. and D. L. Anderson, Theoretical basis of some empirical relations in seismology, *Bull. Seismol. Soc. Am., 65,* 1073-1095, 1975.

Kanamori, H. and J. W. Given, Use of long-period surface waves for fast determination of earthquake source parameters, *Phys. Earth Planet. Inter., 27,* 8-31, 1981.

Kanamori, H. and M. Kikuchi, The 1992 Nicaragua earthquake: A slow earthquake associated with subducted sediments, *Nature, 361,* 714-716, 1993.

Lallemand, S., and X. Le Pichon, Coulomb wedge model applied to the subduction of seamounts in the Japan trench, *Geology, 15,* 1065-1069, 1987.

Masson, D. G., L. M. Parson, J. Milson, G. Nichols, N. Sikumbang, B. Dwiyanto and H. Kallagher, Subduction of seamounts at the Java trench: A view with long-range sidescan sonar, *Tectonophysics, 185,* 51-65, 1990.

Newman, A. V., and E. A. Okal, Teleseismic estimates of radiated seismic energy: The E/M_0 discriminant for tsunami earthquakes, *J. Geophys. Res., 103,* 26,885-26,898, 1998.

Okada, Y., Internal deformation due to shear and tensile faults in a half space, *Bull. Seismol. Soc. Am., 82,* 1018-1040, 1992.

Polet, J., and H. Kanamori, Shallow subduction zone earthquakes and their tsunamigenic potential, *Geophys. J. Int., 142,* 684-702, 2000.

Ruff, L., and H. Kanamori, Seismicity and the subduction process, *Phys. Earth Planet. Inter., 23,* 240-252, 1980.

Satake, K., Mechanism of the 1992 Nicaragua tsunami earthquake, *Geophys. Res. Lett., 21,* 2519-2522, 1994.

Scholz, C. H., and C. Small, The effect of seamount subduction on seismic coupling, *Geology, 25,* 487-490, 1997.

Smith, G. P., and G. Ekström, Improving teleseismic event locations using a three-dimensional earth model, *Bull. Seismol. Soc. Am., 86,* 788-796, 1996.

Smith, G. P., and G. Ekström, Interpretation of earthquake epicenter and CMT centroid locations, in terms of rupture length and direction, *Phys. Earth Planet. Inter., 102,* 123-132, 1997.

Smith, W. H. F., and D. T. Sandwell, Global seafloor topography from satellite altimetry and ship depth soundings, *Science, 277,* 1956-1962, 1997.

Stein, R. S., The role of stress transfer in earthquake occurrence, *Nature, 402,* 605-609, 1999.

Tanioka, Y., Analysis of the far-field tsunamis generated by the 1998 Papua New Guinea earthquake, *Geophys. Res. Lett., 26,* 3393-3396, 1999.

Tanioka, Y., and K. Satake, Tsunami generation by horizontal displacement of ocean bottom, *Geophys. Res. Lett., 23,* 861-864, 1996.

Tsuji, Y., F. Imamura, H. Matsutomi, C. E. Synolakis P. T. Nanang, Jumadi, S. Harada, S. S. Han, K. Arai, and B. Cook, Field survey of the east Java earthquake and tsunami of June 3, 1994, *Pure Appl. Geophys., 144,* 839-854, 1995.

Wessel, P., and W. H. F. Smith, Free software helps map and display data, *Eos Trans. AGU, 72,* 441, 445-446, 1991.

R. E Abercrombie, M. Antolik, K. Felzer, and G. Ekström, Department of Earth and Planetary Sciences, Harvard University, 20 Oxford Street, Cambridge, MA 02138. (Rachel@seismology.harvard.edu; Antolik@seismology.harvard.edu; Felzer@seismology.harvard.edu; Ekstrom@seismology.harvard.edu)

(Received May 12, 2000; revised October 26, 2000; accepted November 3, 2000.)